Applied Catalysis B: Environmental 187 (2016) 30–36

Contents lists available at ScienceDirect

Applied Catalysis B: Environmental

journal homepage: www.elsevier.com/locate/apcatb

An insight on the role of La in mesoporous WO_3 for the photocatalytic conversion of methane into methanol

Katherine Villa[a,*], Sebastián Murcia-López[a], Joan Ramón Morante[a,b], Teresa Andreu[a]

[a] Catalonia Institute for Energy Research (IREC), Jardins de les Dones de Negre 1, 08930 Sant Adrià de Besòs, Spain
[b] Department of Electronics, University of Barcelona (UB), Marti i Franquès 1, 08028 Barcelona, Spain

ARTICLE INFO

Article history:
Received 30 November 2015
Received in revised form 8 January 2016
Accepted 12 January 2016
Available online 15 January 2016

Keywords:
CH_4 conversion
Mesoporous WO_3
Metal doping
Methanol
Photocatalysis

ABSTRACT

One of the great challenges in the photocatalytic oxidation of methane into methanol is to find a suitable catalyst that allows an increase in the selectivity without diminishing the total conversion, since the main feature that rules the yield of this reaction is the overoxidation to CO_2. Ordered mesoporous metal oxides show large surface area and good light harvesting, resulting in efficient catalysts for many photocatalytic applications. With this in mind, a new highly active photocatalyst, La doped mesoporous WO_3, was examined. The production of methanol over WO_3/La was approximately 2 times higher than that of pure WO_3 while the CO_2 rates were significantly decreased, resulting in higher methanol selectivity. This improvement was mainly due to lanthanum contributing to maintaining the mesoporous structure during calcination treatment and increasing the generation of OH groups on the surface of WO_3. Their availability plays a major role in the CH_4 conversion into methanol.

1. Introduction

The large abundance of methane in nature makes it an attractive raw material for obtaining fuels and valuable organic compounds such as formaldehyde, dimethyl ether, acetic acid, etc. Nevertheless, its low reactivity and chemical stability limits its conversion to energy intensive reactions.

Quite recently, considerable attention has been paid to the conversion of methane into methanol under mild conditions by photocatalysis [1–3]. One of the first examples of this photocatalytic partial oxidation in the presence of an electron transfer over WO_3 is presented in [4]. Moreover, Gondal et al. [5] found that in comparison to TiO_2 and NiO, WO_3 showed the largest conversion of methane to methanol. It was explained on the base of this material having a lower conduction band edge that it does not provide a sufficient potential to reduce O_2 to superoxide radical. This reactive radical is one of the responsible for the complete oxidation of products to CO_2. Hameed et al. [6] have shown that the presence of Ag^+ on WO_3 improves the yield of photocatalytic production of methanol by diminishing the charge recombination. Taylor et al. [7] have also studied the performance of different metal doped non-porous WO_3 samples (M/WO_3, M = Cu, Pt, La/Cu and La) on the methane conversion with water at high pressure conditions. Among the samples studied, the La doped catalyst displayed the highest rates of methanol generation. However, there is no explanation about the catalytic role of lanthanum in this improvement.

Recently, we have reported an efficient ordered mesoporous WO_3 catalyst for the selective oxidation of CH_4 with water. In addition, it has been found that the hydroxyl groups adsorbed on the WO_3 surface are chiefly responsible for enhancing the generation of methanol in this photocatalytic reaction [8]. Since basic metals can be used as co-catalysts to promote the formation of these OH groups on the catalysts surface [9], we believe that the modification of the mesoporous WO_3 surface by lanthanum doping should significantly improve the yield and selectivity to methanol in this conversion. Moreover, it has been documented that La helps to maintain the surface area of materials by avoiding particle sintering during calcination treatment, resulting in an enhancement of the activity [10–14].

The aim of this work is to investigate for the first time the performance of an ordered mesoporous WO_3/La catalyst in the photocatalytic conversion of methane into methanol with water in a continuous process. Besides, the effect of La doping on the reactivity and surface properties of WO_3 is also examined in detail to contribute to a better understanding of the enhanced photoactivity of this material.

* Corresponding author.
E-mail address: kvilla@irec.cat (K. Villa).

http://dx.doi.org/10.1016/j.apcatb.2016.01.032
0926-3373/

2. Experimental

2.1. Catalyst preparation

KIT-6 mesoporous silica template with cubic *Ia3d* structure was synthesized in acidic conditions using a mixture of Pluronic P-123 and 1-butanol [15]. Ordered mesoporous WO_3 was prepared by a hard template replicating method as described in our previous work [16]. La doped WO_3 was obtained as follows: the proper amount of 0.1 M $LaNO_3$ solution was added to the ethanolic solution of phosphotungstic acid hydrate (precursor of WO_3) and the resulting mixture was then incorporated into 0.75g of as-prepared KIT-6 silica under stirring. After being dried for 5 h at 100 °C, the obtained powder was calcined for 4 h at 350 °C to eliminate the nitrate, and then further at 550 °C for 6 h to obtain WO_3/La inside the hosting silica. Later, the obtained material was suspended under stirring in a 10 wt% HF solution to remove the KIT-6 silica template. Finally, the La doped mesoporous WO_3 catalyst was separated by centrifugation washed sequentially with water and ethanol and dried at room temperature. Different La loadings of 1.0 and 2.0 wt% were tested, but the highest methanol selectivity was obtained for the catalyst with 1 wt% of lanthanum content (See the Supplementary material, Fig. S1). Then, this study is mainly based on mesoporous WO_3 doped with 1 wt% La, otherwise indicated, this sample is labeled as WO_3/La.

For the gas-solid photocatalytic tests, flat glasses (4.4 cm^2) previously cleaned were used as substrates for the immobilization of the catalysts by spray coating with a commercial airbrush. Prior deposition, suspensions of the as-prepared mesoporous catalysts (5.3 mg/mL) were obtained by sonication in ethanol for 10 min. During and after the spray deposition, the glass substrates were heated at 90 °C for 3 h using a heating plate, in order to improve homogeneity and to assure complete solvent drying. The final amount of immobilized catalyst was found to be 0.7 ± 0.2 mg (determined by weighting the substrates before and after deposition).

2.2. Catalyst characterization

The crystal structure and the optical absorption of the catalysts were characterized by XRD and UV–Vis diffuse reflectance spectroscopy respectively. A Zeiss Auriga FESEM microscope was used to perform scanning microscopy of the samples and TEM images were taken on a Zeiss LIBRA 120 instrument. BET surface area was obtained with a Micromeritics TriStar II apparatus. Raman scattering measurements were performed at room temperature using a LabRam HR800-UV Horiba–Jobin Yvon spectrometer in combination with a solid state 532 nm laser as the excitation source. Since the CO_2 is an acidic gas, the surface basicity of the samples was determined by temperature-programmed desorption of CO_2 (CO_2-TPD) using an AutoChem II 2920 Micromeritics apparatus equipped with a TCD detector. The catalyst was pretreated at 90 °C for 1 h under He flow, cooled to room temperature, and then activated at 250 °C under H_2 flow. Finally, it was exposed to 10%CO_2/He at RT for 2 h by purging with He flow at 35 °C for 45 min. The TPD was run at a heating rate of 10 °C/min from room temperature to 600 °C under He flow. XPS spectra were recorded using a Physical Electronics PHI 5500 spectrometer with a monochromatic X-ray radiation source at 1486.6 eV working at 350 W. All peaks were charge corrected to the adventitious C1s peak at 284.8 eV. TGA analysis was carried out by using a Perkin Elmer TGA 400. Prior to the measurement, the samples were maintained at 35 °C up to stabilization of the initial weight. Then, the samples were heated in air atmosphere from 35 °C to 800 °C (heating rate 5 °C/min).

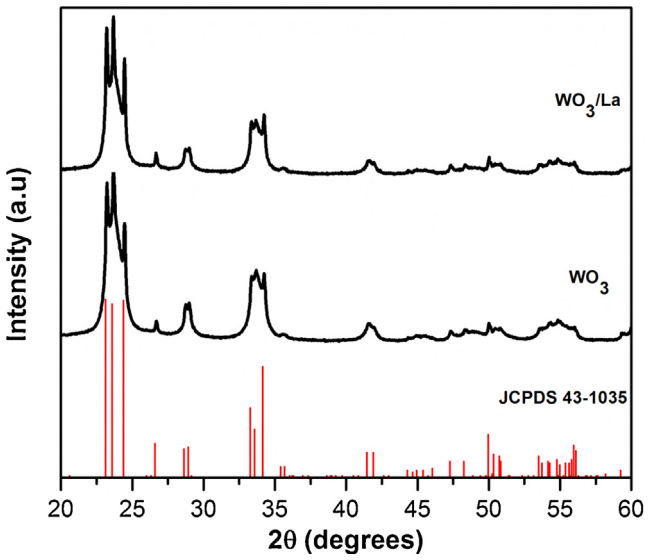

Fig. 1. X-ray powder diffraction spectra of mesoporous WO_3, WO_3/La and the corresponding diffraction pattern of monoclinic phase (0043-1035).

2.3. Photocatalytic setup

The photocatalytic partial oxidation of methane was carried out in a quartz photochemical reactor (Ace Glass) of 500 mL volume equipped with gas inlet and outlet. A medium-pressure mercury lamp (Ace Glass) inside the reactor was used to provide UVC-visible light irradiation. The reaction temperature was maintained at 55 °C by recirculation of cold water in the outer jacket of the lamp. A mixture of methane (4.5 mL min^{-1}) and helium (17.9 mL min^{-1}) was sparged continuously through the photocatalytic reactor. The outlet gas tube was connected to the port valve (with a 0.5 mL loop) of the gas chromatography equipment (GC) to analyze products formation during reaction. In a typical experiment, 300 mL of water (milli-Q) containing 0.3 g of catalyst were placed in the reactor. Prior to illumination, the suspension was magnetically stirred in the dark for 30 min to reach adsorption-desorption equilibrium. After that, the lamp was turned on and gas samples were periodically taken for analysis.

Gas-solid reactions were carried out to evaluate the role of the content of water on the catalyst surface in the selective oxidation of methane to methanol. For this purpose, the same photocatalytic reactor described above, was previously dried at 100 °C overnight to remove any trace of water. Then, the immobilized catalyst was placed inside the reactor under a continuous flow of methane (4.5 mL min^{-1}). This photocatalytic setup is illustrated in Fig. S2. After irradiation, gas samples were periodically analyzed by gas chromatography.

3. Results and discussion

3.1. Catalysts characterization

The XRD patterns of pure and La doped WO_3 are shown in Fig. 1. The diffraction peaks of both samples indicate the presence of the monoclinic structure of WO_3 (JCPDS 43-1035). No crystalline phases related to La or La_2O_3 were detected, probably due to its low concentration. On the other hand, taking into account that the ionic radius of La (1.15 Å) is much larger than the ionic radius of the W (0.64 Å), the former is more likely to be found disperse on the surface of WO_3. The crystal size was estimated to be 12.0 nm and 11.0 nm for WO_3 and WO_3/La, respectively, based on the Scherrer equation. The band gap energy (Eg) of the materials was calculated

Table 1
Surface area, pore volume, wall thickness, energy band gap and CO_2 adsorption capacities of WO_3 and WO_3/La samples.

Sample	Surface area ($m^2\ g^{-1}$)	Pore volume ($cm^3\ g^{-1}$)	Wall thickness (nm)	Band gap (eV)	CO_2 adsorption capacity ($\mu mol\ g^{-1}$ cat)
WO_3	151.0	0.185	6.0	2.7	54.9
WO_3/La	170.7	0.304	5.0	2.6	126.6

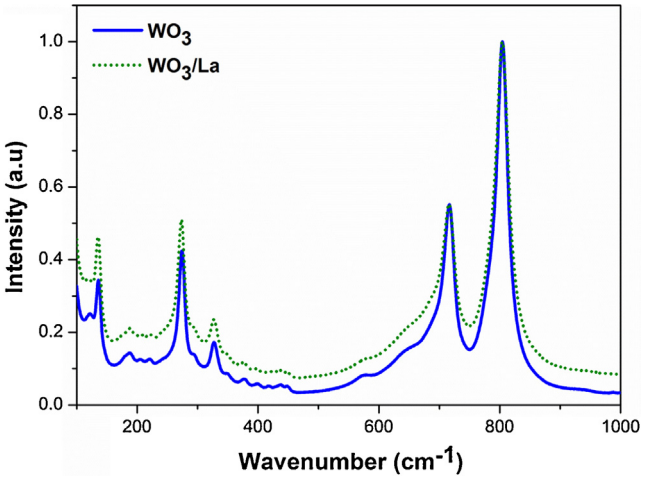

Fig. 2. Raman spectra of mesoporous WO_3 and WO_3/La samples.

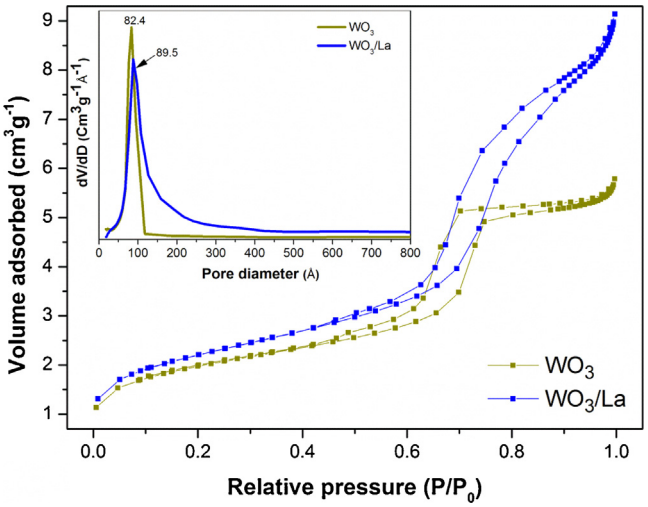

Fig. 3. N_2 adsorption/desorption isotherms and corresponding pore size distribution curves (inset) for mesoporous WO_3 and WO_3/La samples.

from the absorption data by using the Tauc relation (See the Supplementary material, Fig. S3). As shown in Table 1, the estimated E_g values for WO_3 and WO_3/La are in agreement with other values found in the literature for monoclinic WO_3 (~2.7 eV) [17,18]. A red shift in the optical absorption of the pure WO_3 is observed after being doped with lanthanum. Similar results have also been reported for La doped ZnO and TiO_2 [19]. In the latter, it has been attributed to the charge-transfer transition between La^{3+} ion *f* electrons and the TiO_2 conduction or valence band [20].

Fig. 2 illustrates the Raman spectra of the as-synthesized samples. The peaks at 135.0, 274.0, 716.6 and 804.2 cm^{-1} are typical features of the monoclinic structure of WO_3, which is consistent with the XRD results [21]. The lack of the peak at approximately 950 cm^{-1}, attributed to the stretching mode of $W^{6+}=O$ [22], confirms the crystallinity of the catalysts. After La doping, the intensity of the peaks is lower and the two most intense peaks at 716.6 and 804.2 cm^{-1}, corresponding to ν(O-W-O) vibration mode, become wider. For instance, the FWHM of the band at 804 cm^{-1} increases from 29.3 cm^{-1} to 31.5 cm^{-1}. This shows that the La doping causes a distortion of the structure of WO_3, which would be related to the restriction of the grain growth, as evidenced by BET surface area and SEM analysis described below. On the other hand, the Raman bands at 104, 191 and 411 cm^{-1} assigned to La_2O_3 were not observed in the WO_3/La sample, confirming the presence of lanthanum in a disperse phase on the catalyst.

The BET surface area and the pore volume of WO_3 and WO_3/La are shown in Table 1. The WO_3/La sample exhibits a higher surface area and larger pore volume than pure WO_3, resulting in a catalyst with a high adsorption capacity of reactant molecules, which is beneficial for the photocatalytic reaction. Similar observations have been reported for other La doped materials such as Al_2O_3 and $NaTaO_3$ [23,24].

As shown in Fig. 3, both samples exhibit a type IV isotherm which has a characteristic hysteresis loop associated with mesoporous solids. Likewise, the pore size distribution curve (inset) clearly confirms that the uniform pore sizes are in the mesoporous region (20–500 Å).

Surface morphology analyzed by SEM (Fig. 4a and b) reveals particles with irregular shapes and an average of approximate size of 225 nm and 125 nm size for WO_3 and WO_3/La, respectively. These particle sizes are much larger than those obtained previously from the XRD analysis, which evidence the agglomeration of a large number of crystals in both catalysts. The inhibition of grain growth in the doped WO_3 catalyst is probably due to the dispersion of La^{3+} at the interface between grains, hampering its direct contact. Thus, the coalescence of particles and the subsequent decrease of active sites are avoided. Furthermore, small sizes also promote low recombination rates because of the short distance the photogenerated carriers must travel from the bulk to the surface of the catalyst [25].

The TEM images show predominantly well-ordered structures (Fig. 4c and d), indicating that the catalysts are a good replica of the KIT-6 silica template. Compared with the ordered structure of pure WO_3, the WO_3/La catalyst exhibits more defined pores. Besides, the wall thickness calculated from the method described in [26] also evidences thinner wall thickness after doping. This result is in agreement with the increase of the surface area and pore diameter evidenced by the BET analysis discussed above.

Zhang [27] developed a scale of Lewis acidity (Z) using the electronegativity values of elements in valence states. According to this, La^{3+} (Z = 0.852) exhibits a basic character whereas W^{6+} (Z = 3.158) shows a high acidity. Then, CO_2-TPD analysis was performed to determine to what extent lanthanum influences the acidic behavior of WO_3. Fig. 5 shows the CO_2 TPD profiles of WO_3 and WO_3/La. Both samples mainly exhibit the contribution of weak basic sites, however, the CO_2 adsorption capacity of the WO_3/La catalyst is 2.3 times higher than that of pure WO_3, while the increase in the surface area is only 13%. The peak temperature of CO_2 desorption also increases from 86.6 to 112.9 °C, indicating that the strength of the weak basic sites of WO_3 is raised by the addition of lanthanum. According to literature this contribution is assigned to the formation of bicarbonate species from hydroxyl groups ($^-$OH) [28]. The CO_2 adsorption capacities on the samples are listed in Table 1.

Surface analysis of the samples was carried out by XPS to determine the chemical states of La and WO_3. Fig. 6a and b depicts the XPS W4f core-level spectra of WO_3 and WO_3/La samples. The signals were deconvoluted, after a Shirley background, in the two

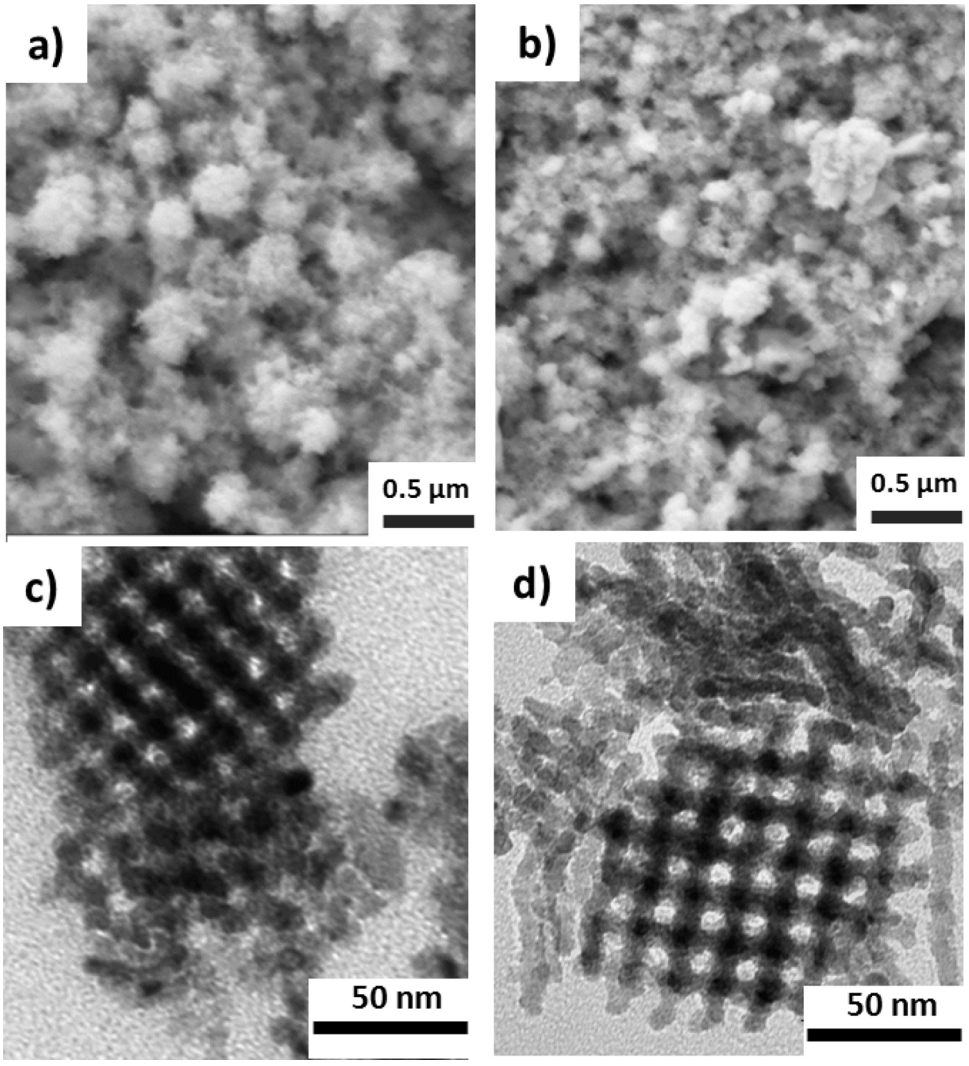

Fig. 4. (a) SEM image of mesoporous WO_3, (b) mesoporous WO_3/La, (a) TEM image of mesoporous WO_3 and (d) mesoporous WO_3/La.

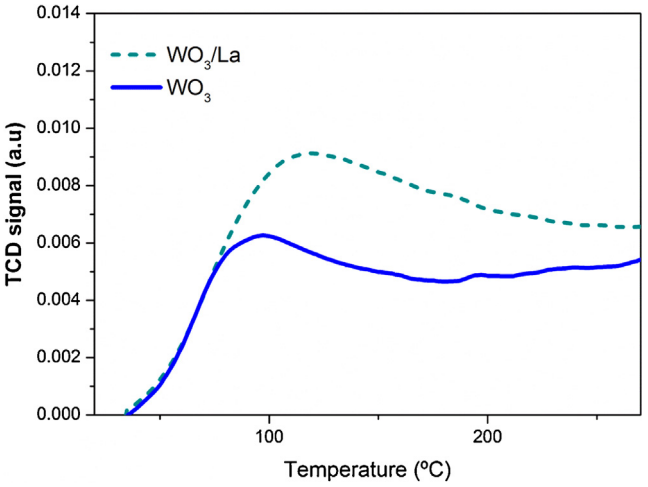

Fig. 5. CO_2-TPD patterns of mesoporous WO_3 and WO_3/La samples.

spin-orbit components $W4f_{7/2}$ and $W4f_{5/2}$, separated by 2.15 eV. The energy position of this doublet corresponds to W^{6+} in WO_3 (Table 2). Compared to pure WO_3, the doped sample presents a broadening of the W4f signals and a slight shift of 0.3 eV towards lower binding energies, which is related to the creation of oxygen vacancies after La doping [29,30].

Table 2
The binding energies of W4f and O1s, and the ratios of O/W and H_2O/O^{2-} for WO_3 and WO_3/La samples.

Sample	W4f	O1s (O^{2-})	O1s (H_2O)	O/W	H_2O/O^{2-}
WO_3	35.8	530.8	533.1	3.0	2.1
WO_3-La	35.5	530.9	533.2	3.7	4.3

The binding energy of the La3d was found to be around 836.4 eV, which is a much higher value than reported for La_2O_3 (833–834.9 eV) [13,31]. According to the literature, this B.E corresponds to La in a dispersed phase with deficiently coordinated La^{3+} ions [32]. Based on the La3d spectrum, the atomic concentration of La in WO_3 was determined to be 0.11% which is a lower concentration than the nominal value (1%). This suggests that La^{3+} cations were well incorporated into the mesoporous structure of WO_3.

Fig. 6c and d illustrates the O1s region corresponding to WO_3 and WO_3/La. Both samples exhibit two contributions at around 530.8 and 533 eV. The first one corresponds to the oxygen atoms in the lattice of WO_3 and the latter at 533 eV is assigned to the water adsorbed on the catalyst surface [33,34]. Nevertheless, there is a remarkable difference in the shape of the spectra of O1s-WO_3 after doping, which is mainly related to a change in the intensi-

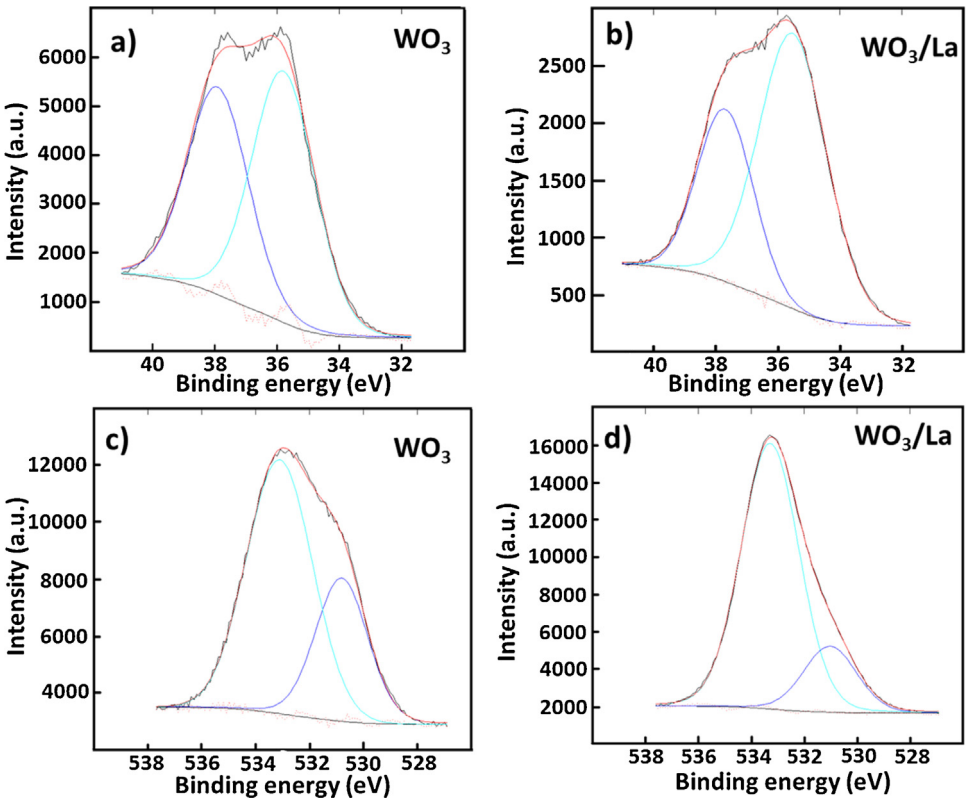

Fig. 6. XPS spectra of (a) W4f core-level of WO_3, (b) W4f core-level of WO_3/La, (c) O1s core-level of WO_3 and (d) O1s core-level of WO_3/La.

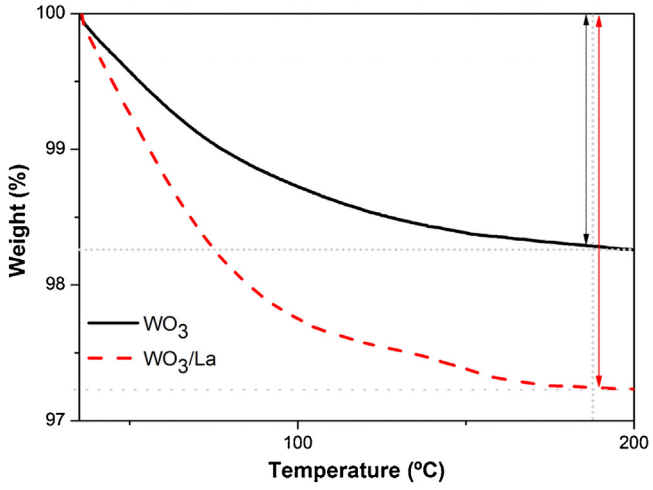

Fig. 7. TGA curves of mesoporous WO_3 and WO_3/La catalysts.

ties of these two contributions. To corroborate this, the H_2O/O^{2-} ratio was determined by the O1s peak (Table 2). It was found that WO_3/La presents a larger amount of adsorbed water on the surface. Accordingly, the calculation of the O/W ratio using only the low binding energy component (contribution of O^{2-}), indicates that the doped sample exhibits an excess of oxygen. This can be explained by considering that the modification of the surface of WO_3 with lanthanum induces the generation of oxygen vacancies, which have the ability to accommodate molecules of water [35].

In addition, TGA analysis was performed to examine the weight loss corresponding to water content in the samples (Fig. 7). Both catalysts show a remarkable loss of weight at temperatures below 200 °C, due to the evaporation of adsorbed H_2O. Once more the WO_3/La shows a higher amount of water (2.8% weight loss) in comparison to pure WO_3 (1.7% weight loss).

3.2. Photocatalytic activity for methanol generation

The photocatalytic activities of mesoporous WO_3 and WO_3/La samples were evaluated on the partial oxidation of methane to methanol with water under UVC-visible light irradiation. The mechanism of the reaction, represented in the scheme below, involves the activation of the catalyst with light energy higher than ~2.7 eV, which leads to the generation of charge carriers able to oxidize H_2O and form $HO^{\bullet}$ radicals [36,37]. Then, these reactive species react with CH_4 molecules to generate methyl radicals, which can combine to generate ethane or react with water to generate methanol and/or other oxygenated compounds [5,38].

Likewise, the photogenerated electrons can carry out the reduction of protons to generate H_2 [5] or can be stored on WO_3 by the presence of H^+ to produce hydrogen tungsten bronze ($H_xW^V{}_xW^{VI}{}_{1-x}O_3$) [39]. In order to discard a possible deactivation of the catalyst during the photocatalytic irradiation, the performance of WO_3 was evaluated in a long-term experiment. As shown in Fig. S4, the methanol generated is maintained almost constant after 7 h of reaction, demonstrating the stability of the material. Furthermore, no changes in the crystalline structure of the catalysts were detected after the photocatalytic tests (See the Supplementary material, Fig. S5). Therefore, the present work is mainly focus on the oxidation pathway.

3.3. Photocatalytic reaction mechanism

$$WO_3 \xrightarrow{h\nu} e^-_{CB} + h^+_{VB}$$

$$e^-_{CB} + H^+ \rightarrow H^{\bullet}$$

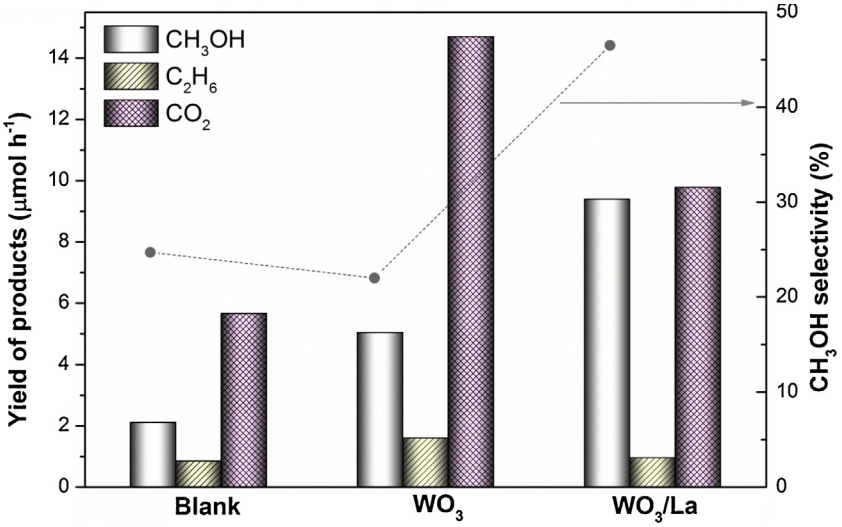

Fig. 8. Yield of products and methanol selectivity in the photocatalytic oxidation of CH_4 on blank, WO_3 and WO_3/La at ~55 °C under UVC–visible light irradiation. Catalyst dosage is 1 g L^{-1}. Data corresponding to 2 h of irradiation in continuous methane flow of 4.5 mL min^{-1}.

$$H^{\bullet} + H^{\bullet} \rightarrow H_2$$

$$h^{+}_{VB} + H_2O_{ads} \rightarrow HO^{\bullet}_{ads} + H^{+}$$

$$h^{+}_{VB} + HO^{-}_{ads} \rightarrow HO^{\bullet}_{ads}$$

$$CH_4 + HO^{\bullet}_{ads} \rightarrow CH^{\bullet}_3 + H_2O$$

$$CH^{\bullet}_3 + CH^{\bullet}_3 \rightarrow C_2H_6$$

$$CH^{\bullet}_3 + H_2O_{ads} \rightarrow CH_3OH + \frac{1}{2}H_2$$

Fig. 8 shows the yield of the major products (CH_3OH, C_2H_6 and CO_2) obtained after two hours of irradiation (from this point the generation of methanol is stable over time). Other minor products such as hydrogen, ethylene, ethanol and formaldehyde were also detected in too low concentration. The contribution of the generated products in the blank experiment (no catalyst), through direct photolysis of water with deep UV lamp ≥185 nm, is much lower than in the presence of catalyst. More importantly, the selectivity to methanol can be enhanced by increasing the amount of catalyst (See the Supplementary material, Fig. S6). This fact demonstrates the need to use a catalyst for increasing the availability of active sites that take part in the formation of methanol during this reaction. Notably, the WO_3/La sample shows a dramatic increase in the generation of methanol and lower values of CO_2 and C_2H_6 than pure WO_3, resulting in a 50% improvement in methanol selectivity.

The positive role played by La on the photoactivity of WO_3 might be explained by considering the following factors. Firstly, La is preventing the collapse of the mesoporous structure after removal of the silica support (KIT-6) during synthesis, resulting in a well-defined ordered structure. Thus, the modified sample shows a slight increase in the surface area and larger pore volume, which contributes to better adsorption capacity of the reactants [40]. Secondly, based on the TGA, XPS and CO_2-TPD results, the role of the La in this photocatalytic conversion would be predominantly related to the increase of adsorbed water on the WO_3 surface and the change of acid-basic properties, in which more OH groups are generated. This is an interesting finding considering that after irradiation, the photogenerated holes can react with these hydroxyl groups and H_2O adsorbed (acting as hole trap), to produce hydroxyl radicals on the catalyst surface.

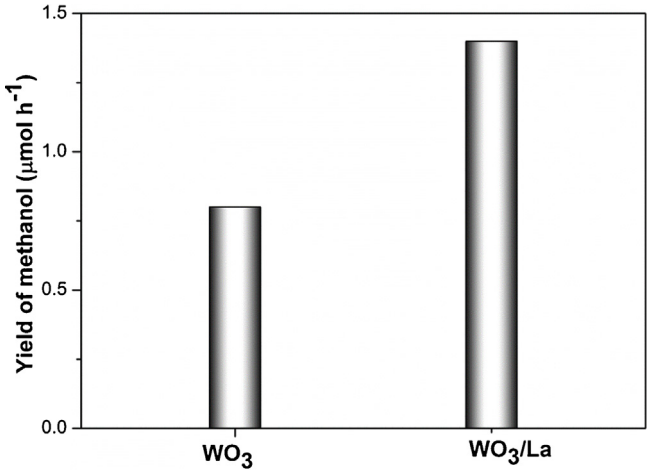

Fig. 9. Yield of methanol in the photocatalytic oxidation of CH_4 on WO_3 and WO_3/La immobilized catalysts, under UVC–visible light irradiation. Data corresponding to 2 h of irradiation in continuous methane flow of 4.5 mL min^{-1}.

In our previous study on the photocatalytic conversion of methane [8], it was found that the modification of the surface of WO_3 with fluoride anions to generate only free hydroxyl radicals leads to a drastic decrease in the generation of methanol, showing the same productivity as the obtained with the blank test. This result provide convincing evidence that the presence of $^{-}$OH groups adsorbed on the catalyst are the key to increase the generation of methanol during this selective oxidation. Thus, as we expected, the enhanced photoactivity of WO_3/La sample is mainly due to La promoting a more rapid and higher generation of hydroxyl radicals adsorbed on the surface than with the pure WO_3.

Complementary to this, we evaluated the photocatalytic performance of the immobilized catalyst in the presence of a continuous CH_4 flow. Fig. 9 depicts the yield of methanol obtained after 2 h of irradiation. Blank tests revealed no products formation in the absence of catalysts. In accordance with the results described above, the yield of methanol generated over WO_3/La sample is about two times higher than that of pure WO_3. Taking into account that in these experiments the only source of hydroxyl radicals comes from the availability of OH groups and water molecules

adsorbed on the catalyst surface, the enhancement on the performance of WO_3/La is directly related to an increase of these species on the catalyst after doping. Once the adsorbed surface OH species are consumed, the yield of methanol decreases (See the Supplementary material, Fig. S7).

It is worth to mention that methanol was the only product detected during these gas-solid reactions, indicating selectivity near 100%. Similar results have been reported in the presence of CH_4/O_2 over MoO_3/Cu [41]. Moreover, considering the large difference between the amount of catalyst used in the liquid-solid and gas-solid tests, if the rates of methanol are normalized per gram of catalyst, the immobilized catalysts show a ~70-fold increase in the yield.

4. Conclusions

In conclusion, it has been found that modifying the surface of WO_3 with lanthanum is a successful approach to significantly increase the selectivity and yield of CH_3OH in the photocatalytic conversion of CH_4. The enhancement in the performance was mainly attributed to the formation of oxygen vacancies that increase the adsorption of H_2O and modification of the basic-acid properties, resulting in higher formation of $^{\bullet}OH$ radicals on the modified catalyst. These results suggest promising applications of mesoporous WO_3/La catalyst in the field of selective oxidation of hydrocarbons under mild conditions.

Acknowledgements

This work was partially supported by the European Regional Development Funds (ERDF, FEDER Programa Competitivitat de Catalunya 2007-2013), the Ministerio de Economia y Competitividad (CSD2009-00050) and the Framework 7 program under the CEOPS project (FP7-NMP-2012-309984).

Appendix A. Supplementary data

Supplementary data associated with this article can be found, in the online version, at http://dx.doi.org/10.1016/j.apcatb.2016.01.032.

References

[1] L. Yuliati, H. Yoshida, Chem. Soc. Rev. 37 (2008) 1592–1602.
[2] Y. Hu, M. Anpo, C. Wei, J. Photochem. Photobiol. A 264 (2013) 48–55.
[3] S. Murcia-López, K. Villa, T. Andreu, J.R. Morante, ACS Catal. 4 (2014) 3013–3019.
[4] R.P. Noceti, C.E. Taylor, J.R. D'Este, Catal. Today 33 (1997) 199–204.
[5] M.A. Gondal, A. Hameed, Z.H. Yamani, A. Arfaj, Chem. Phys. Lett. 392 (2004) 372–377.
[6] A. Hameed, I.M.I. Ismail, M. Aslam, M.A. Gondal, Appl. Catal. A 470 (2014) 327–335.
[7] C.E. Taylor, R.P. Noceti, Catal. Today 55 (2000) 259–267.
[8] K. Villa, S. Murcia-López, T. Andreu, J.R. Morante, Catal. Commun. 58 (2015) 200–203.
[9] S. Noda, M. Nishioka, A. Harano, M. Sadakata, J. Phys. Chem. B 102 (1998) 3185–3191.
[10] K.B. Hewett, L.C. Anderson, M.P. Rosynek, J.H. Lunsford, J. Am. Chem. Soc. 118 (1996) 6992–6997.
[11] T. Kobayashi, T. Yamada, K. Kayano, Appl. Catal. B 30 (2001) 287–292.
[12] J. Nesic, D.D. Manojlovic, I. Andelkovic, J. Mol. Catal. 378 (2013) 67–75.
[13] B.M. Reddy, P.M. Sreekanth, E.P. Reddy, J. Phys. Chem. B 106 (2002) 5695–5700.
[14] Y. Ozawa, Y. Tochihara, M. Nagai, S. Omi, Catal. Commun. 4 (2003) 87–90.
[15] E. Rossinyol, J. Arbiol, F. Peiró, A. Cornet, J.R. Morante, B. Tian, T. Bo, D. Zhao, Sens. Actuators B 109 (2005) 57–63.
[16] K. Villa, S. Murcia-López, T. Andreu, J.R. Morante, Appl. Catal. B 163 (2015) 150–155.
[17] L.J. Zhang, S. Li, B.K. Liu, D.J. Wang, T.F. Xie, ACS Catal. 4 (2014) 3724–3729.
[18] C. Gómez-Solís, D. Sánchez-Martínez, I. Juárez-Ramírez, A. Martinez de la Cruz, L.M. Torres-Martínez, J. Photochem. Photobiol. A 262 (2013) 28–33.
[19] P.V. Korake, R.S. Dhabbe, A.N. Kadam, Y.B. Gaikwad, K.M. Garadkar, J. Photochem. Photobiol. B 130 (2014) 11–19.
[20] Q. Wang, S. Xu, F. Shen, Appl. Surf. Sci. 257 (2011) 7671–7677.
[21] Y. Djaoued, S. Balaji, R. Bruning, J. Nanomater. 2012 (2012) 9.
[22] Y.-S. Huang, Y.-Z. Zhang, X.-T. Zeng, X.-F. Hu, Appl. Surf. Sci. 202 (2002) 104–109.
[23] S.P. Phivilay, A.A. Puretzky, K. Domen, I.E. Wachs, ACS Catal. 3 (2013) 2920–2929.
[24] A. Barrera, S. Fuentes, G. Diaz, A. Gómez-Cortés, F. Tzompantzi, J.C. Molina, Fuel 93 (2012) 136–141.
[25] A. Kudo, Y. Miseki, Chem. Soc. Rev. 38 (2009) 253–278.
[26] P.I. Ravikovitch, A.V. Neimark, Langmuir 16 (2000) 2419–2423.
[27] Y. Zhang, Inorg. Chem. 21 (1982) 3889–3893.
[28] M. León, E. Diaz, S. Bennici, A. Vega, S. Ordóñez, A. Auroux, Ind. Eng. Chem. Res. 49 (2010) 3663–3671.
[29] Y.P. Xie, G.S. Wang, J. Colloid Interface Sci. 430 (2014) 15.
[30] A. Talo, J. Lahtinen, P. Hautojarvi, Appl. Catal. B 5 (1995) 221–231.
[31] L.P. Haack, J.E. Devries, K. Otto, M.S. Chattha, Appl. Catal. A 82 (1992) 199–214.
[32] M. Ferrandon, E. Björnbom, J. Catal. 200 (2001) 148–159.
[33] J.I.M. Szilágyi, B. Fóriz, O. Rosseler, A. Szegedi, P. Németh, P. Király, G. Tárkány, B. Vajna, K. Varga-Josepovits, K. Lászio, A.L. Tóth, P. Baranyai, M. Leskela, J. Catal. 294 (2012) 119–127.
[34] H.Y. Wong, C.W. Ong, R.W.M. Kwok, K.W. Wong, S.P. Wong, W.Y. Cheung, Thin Solid Films 376 (2000) 131–139.
[35] K. Xie, N. Umezawa, N. Zhang, P. Reunchan, Y. Zhang, J. Ye, Energy Environ. Sci. 4 (2011) 4211–4219.
[36] J. Zhang, Y. Nosaka, J. Photochem. Photobiol. A 303–304 (2015) 53–58.
[37] J. Kim, C.W. Lee, W. Choi, Environ. Sci. Technol. 44 (2010) 6849–6854.
[38] C.E. Taylor, Catal. Today 84 (2003) 9–15.
[39] C. Ng, A. Iwase, Y.H. Ng, R. Amal, ChemSusChem 6 (2013) 291–298.
[40] J.S. Church, N.W. Cant, D.L. Trimm, Appl. Catal. A 101 (1993) 105–116.
[41] M.D. Ward, J.F. Brazdil, J. Phys. Chem. 91 (1987) 6515–6521.